ORIGINAL ARTICLE

Wire EDM Parameter Optimization of AlSi10Mg Alloy

Processed by Selective Laser Melting

P. Vaidyaa[1] · J. Jefrin John[1] · M. Puviyarasan[1] · T. Ram Prabhu[2] ·
N. Eswara Prasad[3]

Abstract This work attempts to optimize the multi-objective characteristics of wire electrical discharge machining (WEDM) in SLM-fabricated AlSi10Mg through a hybrid artificial neural network (ANN) coupled genetic algorithm approach. The SLM is unambiguously one of the most effective commercially viable successful additive manufacturing (AM) technologies that have the potential to replace many traditional methods of manufacturing. However, the highly intricate metallic support structures created in SLM are too strong to be eliminated by hands for which precision machining operations such as WEDM are widely employed for post-processing of SLM–AlSi10Mg. The Taguchi experimental design, considering the three most influencing factors, is performed to obtain micro-hardness and surface roughness results. The input factors for optimization are discharge current, discharge voltage, and pulse time-on in the WEDM process. The multi-objective optimization is performed using the ANN coupled GA approach where the ANN model has been generated first and the results of the best model are fed to GA for optimization. For this, five variants of three-layered, multi-perceptron models with feed-forward (BP) neural structures are also developed. The current model is supplemented with a Levenberg–Marquardt algorithm that uses logarithmic sigmoid (logsig) and linear (purelin) transfer functions. Finally, the response values from the best ANN model (3–10–2) are employed for multi-objective optimization using GA. The present study establishes the following optimized process parameters: 12 A discharge current, 42 V discharge voltage, and 12 μs time-on for maximized micro-hardness of 478 VHN and minimized surface roughness of 4.3 μm, both with greater than 98% confidence level. The present study reports briefly phase characterization such as the presence of Si particles, α-Al, and Mg_2Si phases on the recast surface. The surface quality of the optimized specimen exhibits superior surface quality than its other experimental counterparts.

Keywords WEDM · GA-ANN ·
Multi-objective optimization · Surface quality · AlSi10Mg

1 Introduction

The usage of additive manufacturing technologies has gained attention in the past 30 years due to its high progress in manufacturing products with high complexity in design which is practically difficult to manufacture by traditional manufacturing methods [1–4]. This is because AM focuses on manufacturing products in a layer-by-layer fashion [4–6]. In the recent AM practices, laser melting of the layers of powdered metals, often referred to as selective laser melting (SLM), formed in rapid prototyping deserves greater effectiveness in the manufacture of metals and alloys [6]. The SLM involves the melting of powdered metals of diameter 10–100 μm selectively by laser in every layer of the process [3, 4].

The parts produced by SLM are, in fact, superior to their traditional counterparts (casting) in terms of static strength, stiffness, and fatigue strength while maintaining high

✉ M. Puviyarasan
muthupuvi@gmail.com

1   Department of Mechanical Engineering, Panimalar
    Engineering College, Chennai 600123, India

2   CEMILAC, Defence R&D Organization, Bangalore 560093,
    India

3   Defence Materials and Stores R&D Establishment
    (DMSRDE), Kanpur 208103, India

precision in the complex design [3]. Among several Si- and Mg-alloyed Al alloys, the SLM–AlSi10Mg outpaced its traditional counterparts in the aspects of ductility and strength as it evolves an ultrafine hierarchical grain structure in the part [5–15]. The AlSi10Mg alloy is known for high specific strength, stiffness, hardness, and corrosion resistance and is ideal for applications that require a combination of good mechanical properties and low weight such as the aerospace and automotive industry. SLM is one of the proven successful technologies that produce parts with high dimensional accuracy and surface finish than any other AM techniques. In the case of complex part fabrication, it is often needed high strength, support structures to support overhanging features that need to be 'subtracted' in post-processing [16]. These support structures need careful removal to avoid any mechanical damage or inadvertent defects left on the actual part. The wire EDM is an ideal choice to cut the support structures of SLM–AlSi10Mg with greater precision and without leaving any dent on the actual part.

Wire cut electrical discharging machining (WEDM) is a thermal material removal process that makes use of a wire electrode made of thin copper, brass, or molybdenum material by which electrically conductive materials can be cut precisely without the need for cutting force and further finishing process [17–21]. The material removal mechanism of WEDM is similar to the EDM which causes erosion by the series of sparks that arise between workpiece and wire electrode as the tool advances its way [17, 18]. These sparks provide a greater quantum of heat in the temperature range of 8000–12,000 °C initializing significant heating and melting of material at the work–tool interface [17, 18, 21]. The WEDM process is carried out by immersing the workpiece and tool in a continuous supply of dielectric fluid (deionized water) to carry the eroded metal away [17, 20].

The high thermal conductivity of the dielectric fluid results in the rapid cooling of the nascent machined surface resulting in a completely different material microstructure than the parent metal called the recast layer [17]. Moreover, due to the effect of heat, a small portion of the workpiece at about 5 to 25 μm in the vicinity of the machined surface is annealed creating the heat-affected (HA) layer.

The recast layer and the HA layer thickness play a vital role in deciding the property characteristics (such as hardness, fatigue, surface roughness, and corrosion resistance) [18, 22]. Since the micro-hardness depends upon the discharge parameters, an increase in discharge parameters increases micro-hardness. Eventually, these parameters' setting results in a poor surface finish [22]. Even though the material removal mechanism of WEDM and EDM is similar, their functional characteristics differ. WEDM uses

a microprocessor to control the path of the wire electrode which accounts for the remarkable accuracy in the machining of complex parts [17]. Amidst the available machining process on the production floor, WEDM is the most preferable machining process for die making, precision machining, manufacturing of prototypes, aircraft, and dental parts [17]. In addition to that, WEDM is one of the very few metal cutting techniques employed in the post-processing of metal additive manufacturing [16].

It is obvious that either the hardness or surface finish of the product comes out with the compromise of the other. Hence, a particular set of process parameters may fail to obtain high micro-hardness with a good surface finish. This urges a need for mathematical models that relate input parameters with output responses to arrive at an optimum set of process parameters to minimize the surface roughness and maximize the micro-hardness at the least compromise of each other [22].

The hybrid model of the artificial neural network (ANN) coupled genetic algorithm (GA) is one of the recent and widely accepted techniques to find optimal parameters for machining. ANN is a sophisticated mathematical tool inspired by biological phenomena that are recognized for their insane ability to learn and classify data. A neural network is a processing model whose layered structure takes after the organized structure of neurons in the cerebrum, with layers of associated nodes [23]. The ANN models proved to be more robust and accurate in evaluating the value of dependent parameters when compared with RSM models [24]. Many studies concluded that ANN models are more efficient and effective than RSM [23, 24]. The precision of ANN results can be greatly improved by using GA as the optimization tool.

Genetic algorithm (GA) is an optimization tool based on an adaptive heuristic search algorithm inspired by the concept of genetic evolution proposed by Charles Darwin stating 'survival of the fittest.' It uses genetic principles such as selection, mutation, and crossover to arrive at the optimum results [23]. The hybrid model ANN-GA employs ANN as a modeling tool to develop predictive models to predict the relationships between the experimental data sets and GA as an optimization tool to minimize (or maximize) the global population using a fitness function [19, 23]. Additionally, this method is considered both time- and cost-effective since it requires a significantly lesser number of experiments for optimization [23].

The application of hybrid statistical tools (such as GA-ANN, GA-RSM, GA-ANFIS, etc.) in optimization gains importance in recent years due to increased reliability and accuracy in prediction. Since it is a novel approach, there is only limited research carried out in this domain. Deshwal et al. made a comparative analysis on GA-ANN, GA-RSM, and GA-ANFIS in optimizing the process parameters of

FDM and concluded that GA-ANN is the best optimization tool than the other two [24]. Adding to that, the investigations of Yahya et al. and Venkatesh et al. concluded that the ANN model optimized through GA is a potential tool to replace RSM in modeling, optimization, and predicting the results [23, 25].

The primary objective of this research is to develop an effective GA-ANN model to obtain an optimum combination of input parameters of WEDM to cut the support structures of SLM–AlSi10Mg with minimal surface roughness and maximal hardness. This study also provides a detailed analysis of the effect of recast and white cast layers and analyzes the surface morphology through AFM study. Furthermore, an XRD characterization on the machined surface of SLM–AlSi10Mg is carried out to investigate the effect of WEDM on the phase formation after the machining process.

2 Experimental Procedures

2.1 Material and SLM

A cuboidal specimen (100 × 100x 10 mm) was fabricated using the SLM technique with a square print bed of 280 × 280 mm using powdered AlSi10Mg. The powder composition of AlSi10Mg is presented in Table 1.

The test specimens were fabricated in the horizontal direction (parallel to powder bed x–y plane) under the following (Table 2) standard SLM print parameters.

2.2 WEDM

A five-axis CNC-WEDM machine SODICK AG400L was used to carry out the experimental runs with the SLM-printed AlSi10Mg alloy. A brass (copper 60%, zinc 40%) wire electrode of diameter 0.25 mm was used in the WEDM process immersed in deionized water (dielectric fluid). The SLM–AlSi10Mg was cut into nine cuboidal pieces of dimension 12 × 8 × 7 mm. To analyze the impact of the discharge characteristics and pulse duration on the machined specimen, various combinations of input parameters were used according to the L_9 orthogonal array

Table 1 AlSi10Mg chemical composition

Material	Elements (wt.%)					
	Si	Mg	Fe	Cu	Ni	Al
AlSi10Mg	10.8	0.35	0.55	0.05	0.05	Bal

DOE scheme. A pulse-off duration and wire feed rate were kept constant as 14 μs and 3 mm/s, respectively.

2.3 Vickers Hardness Test

The micro-hardness test was conducted on the recast surface of the post-WEDM-processed specimen as per the ASTM E384 standard. The Vickers hardness tester (Model VH150) with a standard diamond indenter (rectangular base pyramid profile) was used for applying a load of 5 kgf for 10 s. Averages of three measurements were considered as the typical hardness of the specimen.

2.4 Surface Roughness Test

The post-WEDM recast surface was tested for surface roughness (Ra) in the Mitutoyo surface roughness tester (Model SJ 210) with a diamond stylus of 10 μm diameter and 0.01 μm accuracy. The surface roughness (R_a) was measured in the direction perpendicular to the tool path according to ISO 1997 standard (sample length: 4 mm). The average value of three experiments was taken as the surface roughness (Ra) of the specimen.

2.5 Metallographic Studies

Samples for microstructure characterization were prepared using the standard metallographic technique. A scanning electron microscope (model: EVO 18 scanning electron microscope) was used to characterize the surface topography of both the white cast and the recast surfaces in the hardest, roughest, and optimum samples. The recast surface of the optimum specimen was examined in the automated high-resolution θ–θ multipurpose X-ray diffractometer (Model: Smart Lab SE, 3 kW X-ray tube, radiation: Cu Kα) with silicon strip detector and vertical-type geometry. The diffraction angle (2θ) was varied between 25 and 95° to obtain XRD spectra to identify the phases present.

2.6 Surface Morphology Studies

The surface morphology of the recast surface (optimum specimen) was analyzed by the atomic force microscope (Model: Park XE7) based on surface observations in the optical microscope. The AFM with SMENA measuring head and vibration isolating system for measuring sample sizes in the nano-scale was used. The measurements were taken with the air contact model using the Si probe of radius 10 nm. The sampling areas of investigation were taken as 15 μm × 15 μm in three locations on the optimum specimen.

Table 2 SLM parameters

Specification/process parameter	Unit	Type/value
Laser beam spot size	mm	30
Atmosphere	–	Nitrogen (99.98% pure)
Laser power (P)	W	370
Layer scan speed (v)	mm/s	1300
Layer thickness (h)	μm	80
Energy density	J/mm^3	49.93
Scanning strategy	–	Rotating stripe
Particle size	μm	90
Volume rate	mm^3/s	5.1
Pre-heat temperature of the base plate	°C	200

3 DOE and Modeling of Hybrid ANN Coupled GA Method

3.1 Taguchi Design of Experiments (DOE)

Taguchi is one of the most profound DOE methods which make use of orthogonal arrays (OAs) to arrive at optimal solutions for a large number of process variables with relatively few numbers of experiments [26–33]. OAs are unique collections (or sets) of arrays which reduces the number of experimental trials to be carried out in a study when compared to conventional DOEs [26–28].

An OA is chosen based on the number of process parameters and their corresponding levels in the experiments [27]. In the present work, three factors—three levels, L$_9$ orthogonal array is taken which reduces the experimental runs from 27 to 9 to find out the best experiment. Signal-to-noise ratio (S/N ratio) is one of the performance functions used in the Taguchi method which is broadly divided into three categories: smaller the better, larger the better, and nominal the better. In this study, the smaller the better and larger the better characteristics are used for responses of micro-hardness and surface roughness (Ra), respectively.

S/N ratio for larger the better characteristic:

$$S/N\ ratio\ (\eta)\ =\ -\ 10\ \log_{10}\left(\frac{1}{n}\sum_{i=1}^{n}\frac{1}{y_{ij}^2}\right). \tag{1}$$

S/N ratio for smaller the better characteristic:

$$S/N\ ratio\ (\eta)\ =\ -10\ \log_{10}\left(\frac{1}{n}\sum_{i=1}^{n}y_{ij}^2\right) \tag{2}$$

where n corresponds to the number of experiments and y_{ij} refers to the response value for the corresponding experiment.

The parameters and levels of parameters are presented in Table 3. The experimental outcomes for the L$_9$ orthogonal array along with the S/N ratio are reported in Table 4.

3.2 ANN Modeling

The key factors that are responsible for the development of an accurate and reliable ANN model are the selection of the best neural architecture, the type of learning algorithm, and the transferring function applied in the hidden and output layers. Adding to that, the number of hidden neurons also plays a vital role in the prediction of results. The ANN model developed for this work is based on a multi-layered perceptron (MLP) which is widely used across investigators to approximate nonlinear relationships among the existing input (independent) and output (dependent) variables [23, 24]. In this research, a feed-forward neural network of backpropagation (BP) is the learning algorithm applied to train the experimental data to develop a predictive model with a three-layer (input, hidden, and output) architecture.

The general design of the MLP neural network is shown in Fig. 1. The training function used in this work is the Levenberg–Marquardt (trainlm) or LM algorithm which is considered the best training algorithm of optimization using the GA-ANN technique [25]. The BP technique is extensively used by researchers because of its high reliability in modeling and optimizing the functions [23, 34–36]. The selection of transfer functions used in the input and output layers is important as they affect the learning rate and overall performance of the ANN model [23, 35]. The transfer function used in this work is logarithmic sigmoid in the hidden layer and linear (purelin) in the input and output layers. The number of neurons in the input and output layers is fixed by the number of input process parameters and the number of output responses, respectively [24, 37].

The general form of neural architecture is labeled as 3-x-2 (three input neurons representing the WEDM process parameters (discharge voltage, current, and time-on) and two output neurons (micro-hardness and surface roughness)), where x is the total number of neurons in the hidden layer used in ANN modeling. Firstly, the number of hidden layers used in this investigation is chosen as one, since it is considered effective in solving the majority of the problems to avoid issues like overfitting as a result of the application of multiple hidden layers [23, 38]. Secondly, it is important to select the number of neurons in the hidden layer. This is because if the number of hidden neurons is too low to cope up with the complexity of the problem it forms an under-fitted model. On the other hand, the redundant number of hidden neurons results in the degradation of the network capability when it is trained based on

Table 3 WEDM process parameters and their levels

Level	Discharge current (Amps)	Discharge voltage (Volts)	Pulse on-time (μs)
1	12	42	10
2	13	44	11
3	14	46	12

training data alone [23, 39]. The number of neurons in the hidden layer is usually obtained by the hit-and-trial method, and the optimized number of hidden neurons is achieved by iteration.

The optimum number of neurons in the hidden layer is obtained by analyzing the performance of the neural architecture based on the regression value. For this purpose, five neural architectures are developed to train, test, and validate the test data with the number of neurons in the hidden layer varying from 8 to 12. The objective is to find out the best neural architecture (the one with an optimum number of hidden neurons) with the highest regression rate among the available variants (neural architectures varying from 8 to 12 hidden neurons). For this purpose, the neural network tool (nntool) available in MATLAB R2018a is used to train the network model to model and analyze the neural networks [24]. Mean relative error (MRE), root mean square error (RMSE), and regression coefficient (R^2) are computed for every ANN model to evaluate their performance based on which the best model is selected [40]. The following are equations of MRE, RMSE, and R^2.

$$\text{MRE}(\%) = \frac{1}{n}\sum_{i=1}^{n}\left|100\frac{t_i - o_i}{t_i}\right|. \tag{3}$$

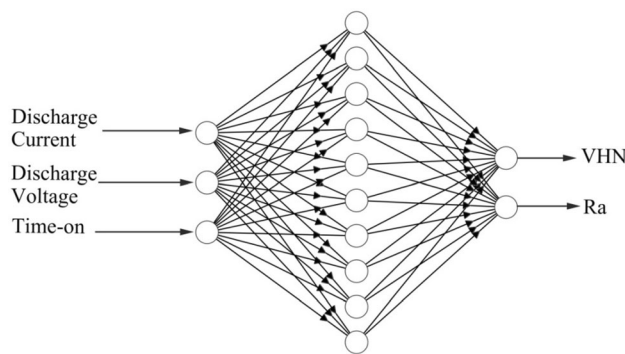$$\text{RMSE} = \sqrt{\frac{1}{n}\sum_{i=1}^{n}(t_i - o_i)^2}. \tag{4}$$

Fig. 1 ANN network diagram

$$R^2 = 1 - \left(\frac{\sum_{i=1}^{n}(t_i - o_i)^2}{\sum_{i=1}^{n}(o_i)^2}\right). \tag{5}$$

Here, n is the number of experimental data, 'o' is the predicted response data, and 't' is the actual response.

3.3 Optimization using Evolutionary Genetic Algorithm

The evolutionary genetic algorithm can be used to optimize the ANN model which has the best neural architecture obtained from the previous steps. For this, the GA solver in the optimization toolbox of MATLAB R2018a is used in this research. Instead of working on the decision variables, GA works on the chromosomes of the existing population. Every chromosome consists of all decision variables in the form of an objective function [28].

GA begins by creating an initial population of chromosomes whose fitness function is determined by the objective function of the problem (multi-objective optimization). Then, the chromosome with the best fitness function is propagated as a parent to form the next generation. This is called the 'selection.' The crossover is a

Table 4 L₉ Orthogonal array with responses

Experiment no.	Discharge current	Discharge voltage	Pulse on-time	Surface roughness	S/N ratio (smaller the better)	Micro-hardness	S/N ratio (larger the better)
	(Amps)	(Volts)	(μs)	(Ra)	(dB)	(VHN)	(dB)
1	12	42	10	4.65	− 13.33	416	52.38
2	12	44	11	4.47	− 13.01	441	52.89
3	12	46	12	4.44	− 12.95	472	53.48
4	13	42	11	4.55	− 13.16	438	52.83
5	13	44	12	4.67	− 13.39	518	54.29
6	13	46	10	4.39	− 12.85	486	53.73
7	14	42	12	5.18	− 14.29	442	52.91
8	14	44	10	4.84	− 13.70	435	52.77
9	14	46	11	4.52	− 13.10	428	52.63

principle of GA by which an opportunity is created to facilitate the selected chromosomes to produce a new one. The offspring is 'mutated' by changing some of their genes. The optimal solution is brought out by creating versatility in the new generation by applying mutation while moving from the existing population [28]. GA can optimize non-differentiable, discontinuous, and highly nonlinear objective functions in several iterations until it reaches the value of predefined maximum generation (i.e., 500 in this study) [28, 41].

4 Results and Discussion

4.1 Analysis of Statistical Significance

Analysis of variance (ANOVA) is a method widely used by investigators [23, 26, 27] to evaluate the statistical significance of the decision variable in any process. In this work, ANOVA is performed to determine how significant are the process parameters (discharge current, discharge voltage, and pulse time-on) of the WEDM process influencing the responses of micro-hardness (VHN) and surface roughness (Ra). Here, the ANOVA is performed based on the S/N value obtained in the previous section. In ANOVA, Fischer's test (F test) is the ratio of the mean sum of squares due to regression to mean sum of squares due to error.

The F value plays a major role in determining the adequacy of the parameter. Tables 5 and 6 depict the ANOVA for micro-hardness and surface roughness along with the individual parameter contribution.

The ANOVA of the WEDM process parameters clearly illustrates that all the process parameters are statistically significant at 95% of confidence for multi-objective responses of micro-hardness and surface roughness.

4.2 Multi-Objective Optimization using Hybrid GA-ANN Method

4.2.1 Training of ANN Model

The modeling of the ANN architecture in MATLAB R2018a (MathWorks Inc.) is briefly discussed in the previous section. The neural networks from 8 to 12 hidden neurons in the hidden layer are tested for their accuracy in predicting the responses of micro-hardness (VHN) and surface roughness (Ra) of the SLM–AlSi10Mg specimen. The ANN parameters for training data are depicted in Table 7.

The best neural architecture needs to have the least MRE, RMSE, and the highest regression coefficient (R^2) to provide the best prediction results among other neural networks [23]. Table 8 shows the MRE, RMSE, and R^2 for

neural architectures ranging from 8 to 10 hidden neurons. Figure 2a–c illustrates graphical values of MRE, RMSE, and regression values obtained from all the five ANN models.

It is evident that the ten hidden neuron structures show balance in the results of all the performance metrics (MRE, RMSE, R^2). So, it is obvious that the neural network with ten hidden neurons in the hidden layer is the 'best fit' for the complexity of the optimization problem without any under-fitting and overfitting issues. Hence, the neural architecture 3–10–2 (three neurons in the input layer, ten neurons in the hidden layer, two neurons in the output layer) is used for further optimization using a genetic algorithm (GA). Figures 3, 4, and 5 represent the complete configuration and performance of 3–10–2 ANN architecture with training, testing, and validation results.

4.2.2 Configuring GA to Optimize the Best ANN Model

The predicted results are fed to the GA solver called 'gamultiobj' available in the Optimization toolbox in MATLAB-R2018a in the form of a fitness function. Fitness functions are nothing but mathematical models in terms of coded factors to predict responses. This fitness function is generated by fitting general linear model in Minitab R19 using the results of the 3–10–2 ANN model.

The fitness function of micro-hardness is:

$$y(1) = 137 - 2.36 \times x(1) + 0.53 \times x(2) + 28.95 \times x(3) \tag{6}$$

The fitness function of surface roughness is:

$$y(2) = 3.20 + 0.0632 \times x(1) + 00.0233 \times x(2) - 0.0380 \times x(3) \tag{7}$$

where $y(1)$ and $y(2)$ refer to the responses of micro-hardness and surface roughness, respectively. $x(1)$, $x(2)$, and $x(3)$ correspond to process parameters of discharge current, discharge voltage, and pulse time-on.

The multi-objective criterion for GA is chosen as VHN (micro-hardness) to maximize and surface roughness (Ra) to minimize. The ranges for experiments are fixed as (12 42 10) for minimum and (14 46 12) for maximum. For this optimization problem, the tournament is applied as a selection method to designate how GA selects parent chromosomes for successive generations. The computational parameters listed in Table 9 provide the values used in GA optimization and the corresponding values used in this optimization problem.

In a population of 50, two of them are fixed as elite counts that pass from the initial population to the next generation and 0.8 and 0.2 are the crossover fraction and

Table 5 ANOVA for micro-hardness

Factor	Process parameters	Degrees of freedom	Sum of squares	Mean square	F-test	Contribution in %
A	Discharge current	2	1.229	0.615	36.12	41.63
B	Voltage	2	0.701	0.350	20.58	23.72
C	Pulse time-on	2	0.989	0.495	29.07	33.50
Error	Error	2	0.034	0.017		1.15
Total	Total	8	2.953			100

Table 6 ANOVA for surface roughness

Factor	Process parameters	Degrees of freedom	Sum of squares	Mean square	F-test	Contribution in %
A	Discharge current	2	0.680	0.340	28.06	42.20
B	Voltage	2	0.601	0.301	24.83	37.34
C	Pulse Time-on	2	0.305	0.153	12.61	18.96
Error	Error	2	0.024	0.012		1.50
Total	Total	8	1.611			100

Table 7 ANN parameters for training data

Sl. no.	ANN parameters	Values
1	Network configuration	03–10–02
2	Number of hidden layers	1
3	Number of hidden neurons	10
4	Transfer function used	Logsig (sigmoid)
5	Number of epochs	500
6	Learning factor	1%
7	Momentum factor	90%
8	Training	Trainlm
9	Max-fail	500

Table 8 ANN network outputs

	Number of neurons in the hidden layer				
	8	9	10	11	12
MRE	4.964	4.244	3.635	3.049	3.965
RMSE	21.550	12.800	11.888	27.283	19.048
R^2	0.9950	0.9970	0.9967	0.9936	0.9955

rate of mutation, respectively. The results of the genetic algorithm show that the optimum conditions for WEDM with minimized surface roughness (Ra) of 4.44 μm and maximized micro-hardness (VHN) value of 478 VHN are

discharge current of 12 A and discharge voltage of 42 V and pulse time-on of 12 μs. A confirmation test was conducted based on the optimized process parameters, and the experimental outcomes are 4.39 μm and 492 VHN, which shows that they closely agree with the predicted results from the GA-ANN model.

4.2.3 Microstructural Analysis

The magnitude of temperature at the workpiece—tool (wire) interface during the WEDM process is typically above the melting point of Al alloys [22, 42]. The dielectric fluid is supplied at a rate so that it should ideally wash the molten metal away from reaching the machined surface to avoid re-solidification of molten metal to the parent metal. But practically, the dielectric fluid cannot wash away all molten material from reaching the machined surface. The unwashed molten metal then rapidly solidifies as a result of a high-temperature gradient existing between the machining interface and dielectric fluid (room temperature) forming a 'recast' layer over the machined surface which is comparatively harder than the un-machined surface [43, 44]. The increase in micro-hardness is because of the ultrafine grain structure formed in the recast layer due to the drastic solidification rate at the machined surface [43, 44]. To gain an understanding of this layer, the hardest, roughest, and optimum specimens were selected and compared for the microstructure. The SEM micrographs of the white cast layer and recast layer of SLMed AlSi10Mg are presented in Figs. 6, 7, 8, 9, 10, and 11.
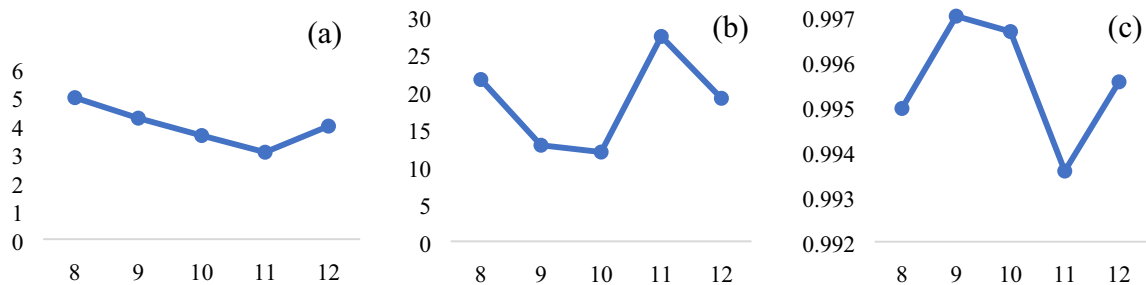
Fig. 2 Variation of **a** MRR, **b** RMS, and **c** regression values with number of neuron structures
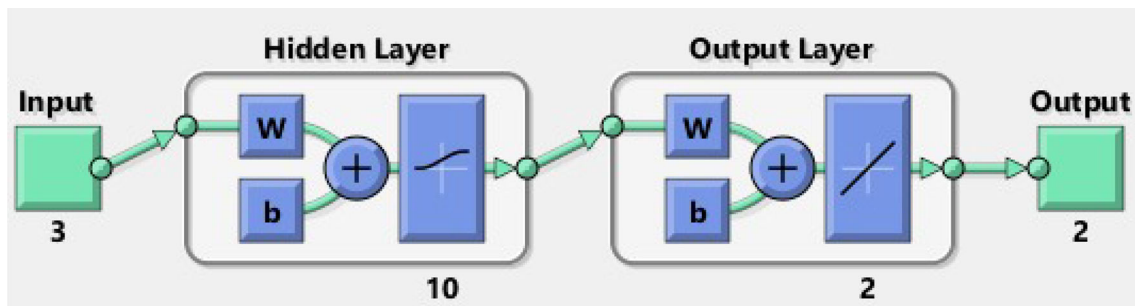

Fig. 3 ANN architecture topography with the transfer function of the logarithmic sigmoid (logsig) for hidden layer and linear (purelin) for the output layer

The thermal energy discharged during the WEDM process creates heat-affected zones (HAZ) in the specimen proportional to the magnitude of the electric discharge energy. The HAZ is the region underneath the white layer (recast layer) affected by the heat transfer from the white layer. The HAZ can be classified into a hardened layer, followed by the annealed layer, and can be viewed from the surface perpendicular to the recast layer. The recast layer can be seen as a thick white line at the machined edge called 'white cast' or 'white layer,' typically 4 μm in thickness [43]. The white layer consists of ultrafine α-Al grains with fine Si particles decorated along the grain boundary. Further, the XRD results confirm the presence of fine Mg_2Si precipitates in the white layer, as shown in Fig. 12. Fine Mg_2Si precipitates and refined microstructure result in very high hardness (518 VHN). The annealed regions experience significant α-Al grain growth and Si particle coarsening due to the heat transfer, whereas a thin layer just below the white layer, i.e., hardened layer experiences little grain or particle coarsening [43, 44]. This explains the hardness difference between the hardened (435 VHN) and annealed (281 VHN) layers. The explanation on how the hardened and annealed layers are developed is given in detail by Hassan El-Hofy [44]. The white layer thickness (WLT) and the HAZ (hardened and annealed layers) are the direct function of discharge energy emitted and the time for which it stays in the wire electrode during the process. The zone below the machined surface will be annealed to produce the white layer. The depth of the annealed layer ranges from 50 to 200 μm for the finish and rough cutting rates, respectively [22, 29–32, 45]. Figures 6, 7, and 8 show the SEM images of the white cast layer. The representation of the white cast layer, followed by the hardened and annealed layer on the recast surface, is shown in Fig. 6a.

Figure 6b, c shows the hardest specimen (518 VHN) with a surface roughness of 4.67 μm. It can be noticed that the hardest specimen has thick bands of white (15.41 μm), hardened (86.9 μm), and annealed (114.43 μm) layers as compared to the least hard (soft) specimen. Hence, the present study shows that micro-hardness is directly proportional to the HAZ layer thickness near the white cast layer. As the HAZ is a function of pulse time-on and discharge variables, the hardest specimen has the highest discharge voltage of 44 V and pulse time-on 12 μs generating more heat that affects more thickness of the parent material and creates a wide HAZ. On the other hand, Fig. 7a, b shows the roughest specimen (Ra = 5.18 μm) with micro-hardness 442 VHN that uses the lowest discharge current of 12 A, discharge voltage of 42 V, and pulse time-on of 10 μs generating less heat when compared to the hardest specimen. The average values of HAZ are found to be 76.6 μm for the hardened layer and 104.5 μm for the annealed layer. Also, at constant pulse time-off of 14 μs, the heat dissipation rate of the least hard (soft) specimen is higher than the hardest specimen

Fig. 4 ANN regression coefficient of experimented vs predicted values for **a** training, **b** testing, **c** validation, and **d** all a–c together
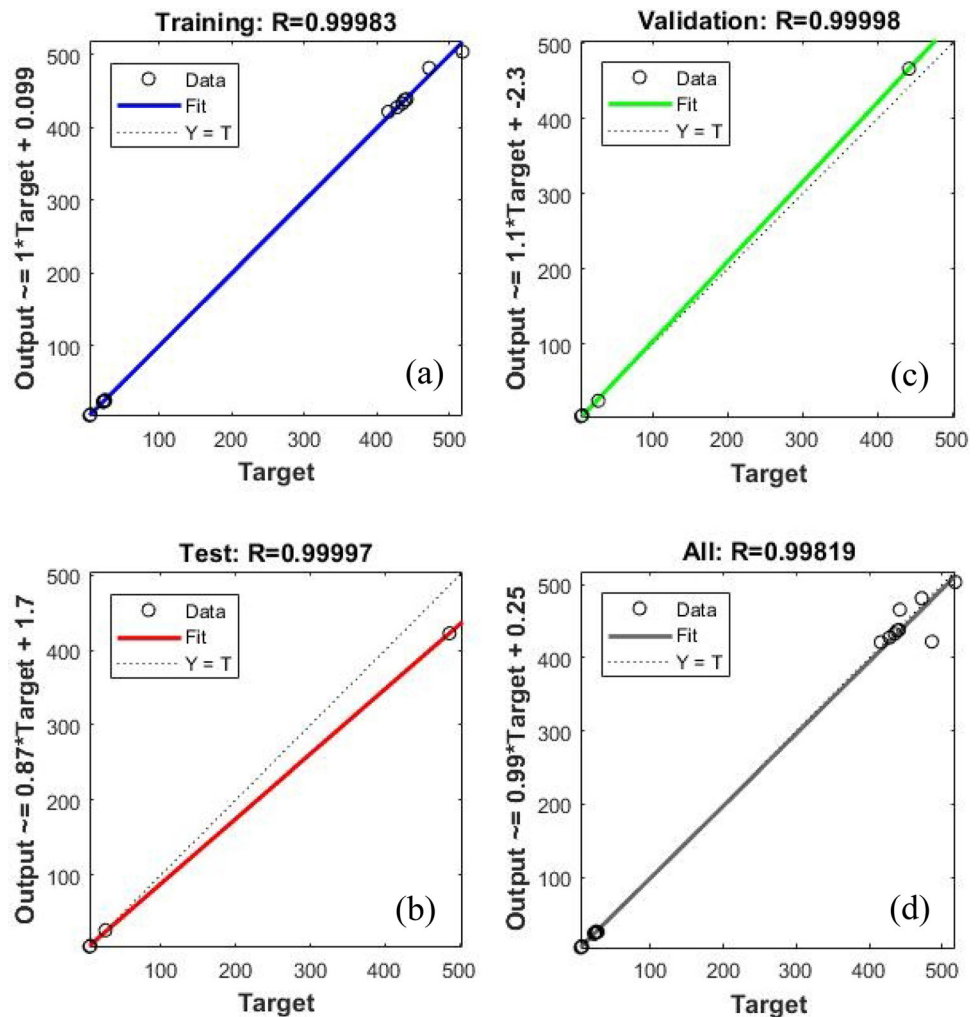
resulting in less HAZ. This variation in heat generated and heat dissipation rate have resulted in variation in the micro-hardness of the specimens. Figure 8a, b shows the SEM images of the optimum specimen. The average thickness of the white layer is found to be 9.7 μm which is lesser than the other specimens. The reduced white layer thickness results in enhanced surface characteristics with a lesser Ra value of 4.39 μm and a micro-hardness of 492 VHN. The HAZ of 53.47 μm of hardened layer and 87.3 μm of an annealed layer is obtained from discharge current of 12 A, discharge voltage of 42 V, and pulse time-on of 12 μs. The lowest discharge current and voltage results in reduced HAZ and white layer thickness which is accounted for a reduction in surface roughness and the highest pulse time-on results in improved micro-hardness. However, the micro-hardness of the optimum specimen may not be of the highest value. The overall multi-objective function compromises only a 6% penalty in the micro-hardness for surface quality (reduced surface roughness) improvement of about 15%.

The recast SEM images (Figs. 9, 10, 11) reveal that the post-machined surface is smooth with few surface defects such as craters, asperities, spherical nodules, pockmarks, debris, and cracks. These surface defects are usually caused by thermal stresses generated due to the rapid cooling of molten metal in the vicinity of the machined surface. The micro-craters (Fig. 9a) are formed as a result of the impact created by spark explosion. Due to this, the micro-melted pool is eroded from the machined surface [43]. These eroded micro-droplets of molten metal then rapidly solidify above the recast surface, forming numerous irregular-shaped microscale asperities, which are shown in Figs. 9b and 10a.

The formation of micro-cracks (Fig. 10b) occurs during the pulse time-on in the WEDM process. From the recast surface analysis, it is clear that the surface defects are more prominent in the specimen with the highest discharge current and time-on with the lowest discharge voltage. Micro-cracks are formed due to the high thermal stresses induced by the high-temperature gradient at the interface.

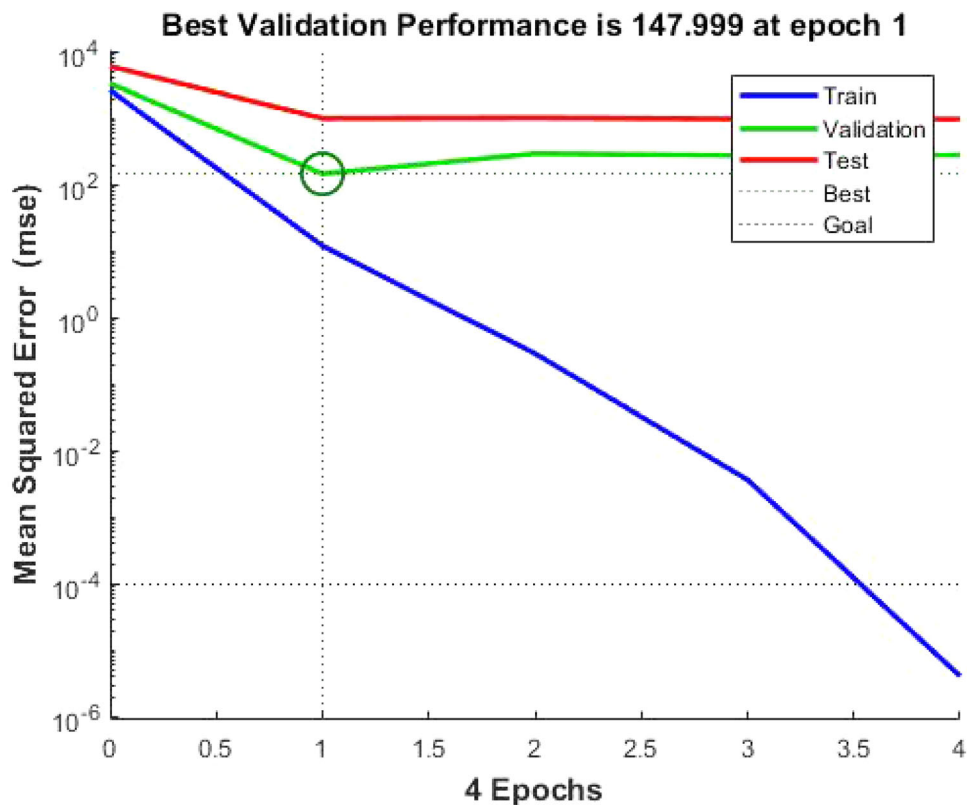**Fig. 5** ANN validation and performance plot for the 3–10–2 model

Table 9 GA Computational parameter of multi-objective optimization

GA computational parameters	Values
Population size	50
Elite count	2
Crossover fraction	0.80
Fitness scaling function	Rank fitness scaling
Direction for migration	Forward with migration fraction set at 0.2
Mutation function	Adaptive feasible
Creation function	Feasible population
Selection function	Tournament

When the magnitude of the thermal stress surpasses the maximum strength limit of AlSi10Mg, the crack develops [46]. In the roughest specimen (Fig. 10a, b), the presence of the micro-cracks and debris on the recast surface increase the surface roughness (Ra). The micro-cracks may cause premature failure of the specimen if they are irregularly distributed in the recast surface, particularly when machined at 14 A discharge current and 12 μs pulse time. The cracks are not getting removed after post-processing (such as polishing and finer finishing) of the WEDM process. Micro-cracks are also responsible for the

reduction of fatigue resistance and tribological properties such as wear resistance [22]. Debris is vertical projections of re-solidified micro-droplets of molten AlSi10Mg found. The optimum specimen (Fig. 11a, b) reports reduced surface defects compared to others. The improvement in the surface properties is because of reduced discharge current and voltage of 12 A and 42 V, respectively. Moreover, for the optimum specimen, the micro-cracks are absent.

4.2.4 XRD

The recast surface of the optimum specimen was analyzed using XRD to understand the phases formed. Figure 12 shows the XRD plot of the recast surface of post-machined SLM–AlSi10Mg. The sharp peaks reveal the high crystalline nature of the AlSi10Mg alloy. The diffraction angles of 39.82, 46.02, 66.3, 79.34, and 83.52 degrees identify as α-Al. The smaller peaks corresponding to 2θ values of 48.65, 58.35, and 89.16 correspond to primary Si particles in the alloy. Further, the peak at 30.57° diffraction angle shows the presence of Mg_2Si (magnesium silicide) precipitate in the alloy. Since Mg_2Si is the hardest phase, its precipitation on the recast surface increases the micro-hardness of the specimen.

It is noted that the deposition of wire electrode material (Cu–Zn alloy) is not observed in the recast surface of post-
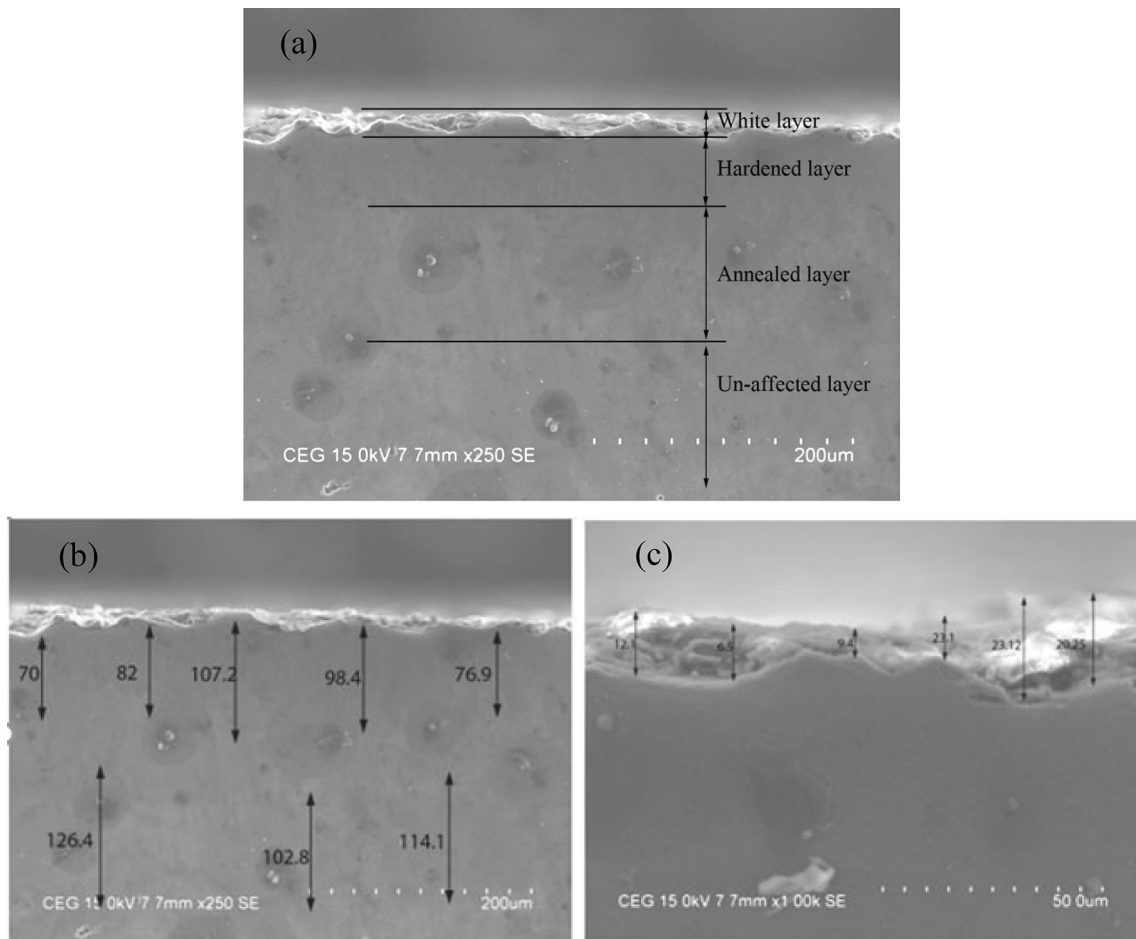
Fig.6 a White layer and HAZ, i.e., hardened and annealed layers representation; WEDM parameters: 13 A, 44 V, 12 μs, b HAZ of highest hardness at 250x: 13 A, 44 V, 12 μs, c white cast layer of highest hardness at 1000x: 13 A, 44 V, 12 μs
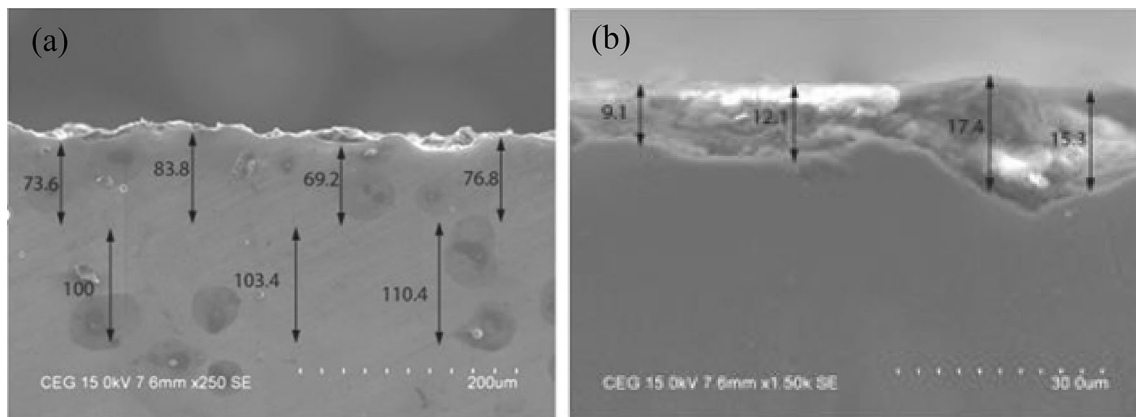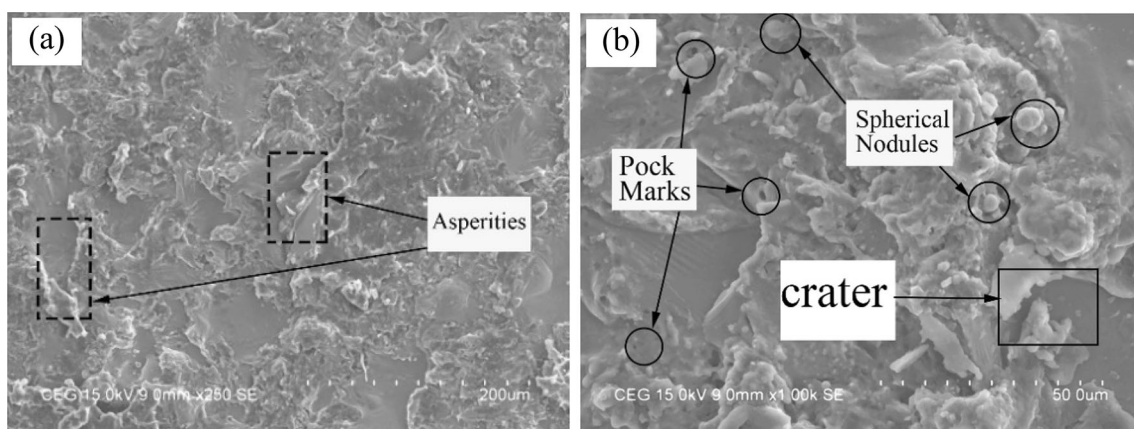

Fig. 7 a HAZ of highest roughness at 250x: 14 A, 42 V, 12 μs, b white cast layer of highest roughness at 1500x: 14 A, 42 V, 12 μs

machined SLM–AlSi10Mg. Hence, it is proposed that the optimum parameters provide not only a good surface finish and higher micro-hardness but also a clean surface free from any traces of the wire electrode material deposition.

4.2.5 Surface Topography

The surface topology of the optimum specimen was analyzed in three different locations in the recast surface to study the effect of process parameters on surface integrity. The location where the AFM analysis is done is depicted in
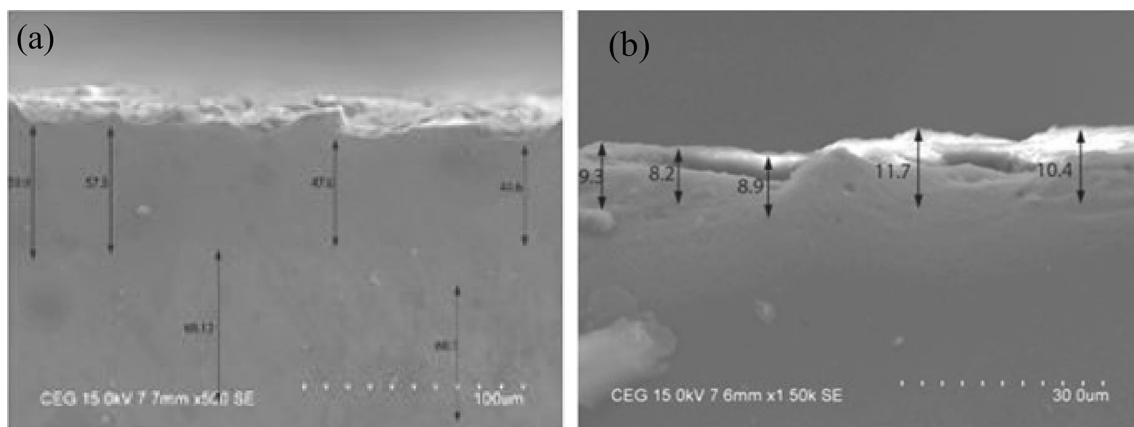
Fig. 8 **a** HAZ of optimum by GA-ANN at 500x: 12 A, 42 V, 12 μs, **b** white cast layer of optimum by GA-ANN at 1500x: 12 A, 42 V, 12 μs

Fig. 9 **a** Recast layer of highest hardness at 250x: 13 A, 44 V, 12 μs, **b** recast layer of highest hardness at 1000x: 13 A, 44 V, 12 μs
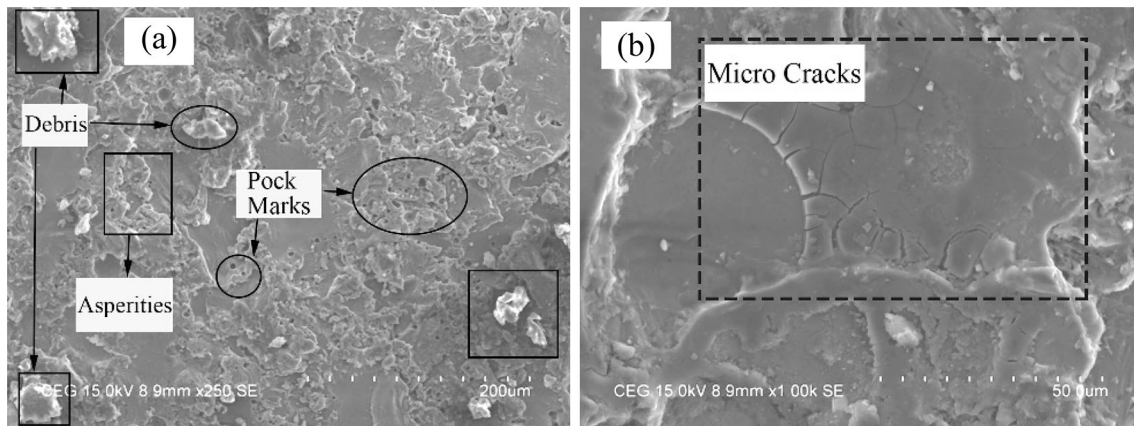

Fig. 10 **a** Recast layer of highest roughness at 250x: 14 A, 42 V, 12 μs, **b** recast layer of highest roughness at 1000x: 14 A, 42 V, 12 μs

Fig. 13. Figures 14, 15, and 16 illustrate the 2D AFM micrographs and their corresponding 3D surface topology taken at locations 1, 2, and 3, respectively. The contrast variation in color denotes the variation in the altitude of the surface where the darker is the deeper region and the brighter is the elevated region. The AFM study shows that surface integrity varies in different locations of the WEDMed surface.

It can be noticed that the value of nano-surface roughness (Ra) increases as it moves deeper into the recast layer away from the periphery to the maximum value at its center. The process parameters of the optimum specimen
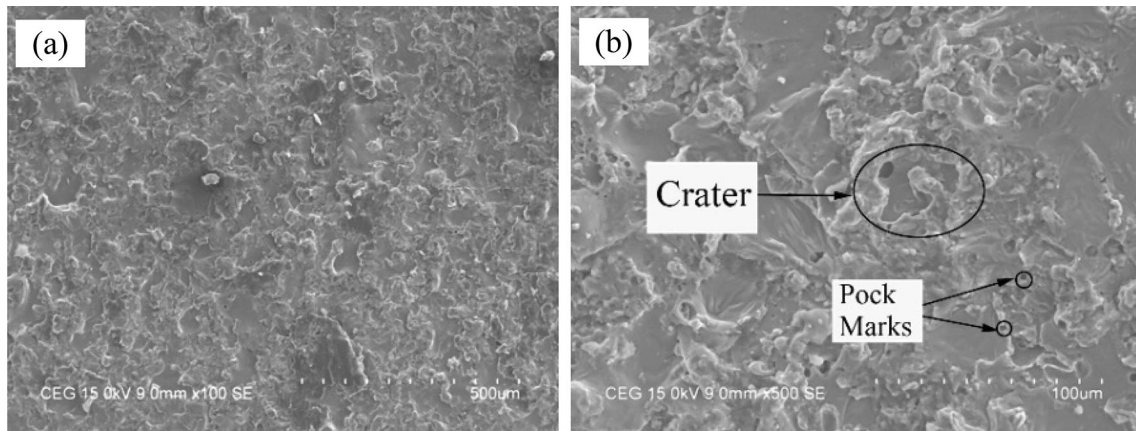
Fig. 11 **a** Recast layer of optimum by GA-ANN at 100x: 13 A, 44 V, 12 μs, **b** recast layer of optimum by GA-ANN at 500x: 13 A, 44 V, 12 μs
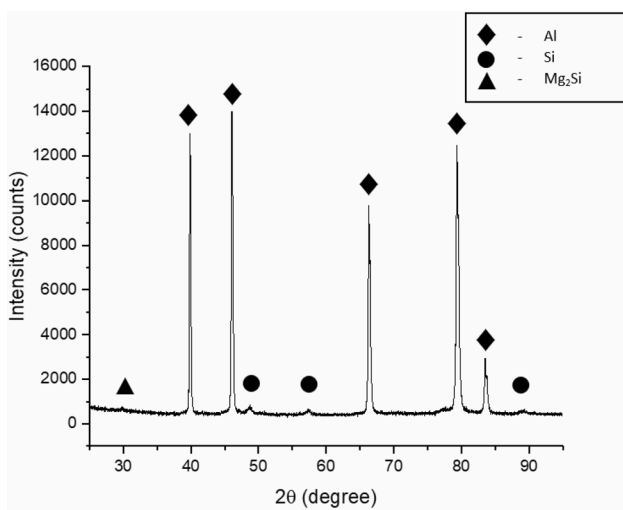

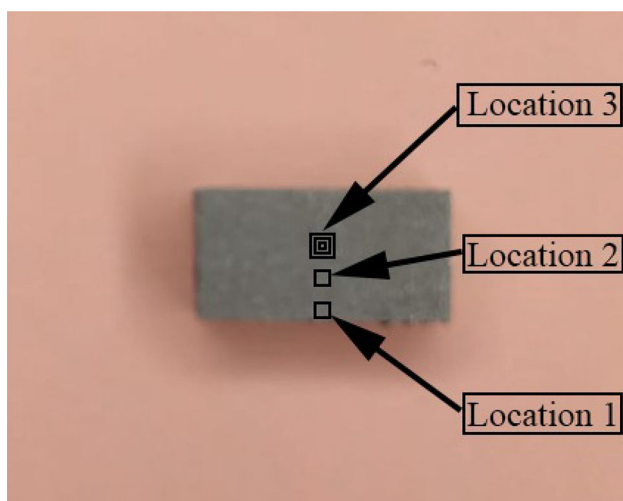**Fig. 12** XRD analysis at the recast layer

Fig. 13 Location of AFM images in the optimum specimen: 13 A, 44 V, 12 μs

are 13 A, 44 V, and 12 μs, respectively. At location 1, the value of surface roughness (Ra) is 46 nm. This is because the areas of heat dissipation are high, resulting in higher heat dissipation when compared to other locations. A part of the heat dissipates through the recast surface and another part escapes through the surface perpendicular to the recast surface (including white cast surface). But location 3, which is at the center of the recast surface, has a very less heat dissipation rate due to the less area of heat dissipation. So, the effect of heat will be the highest in location 3 and lowest in location 1. This resulted in poor surface quality (highest surface roughness 93 nm) in location 3 and the best surface quality in location 1. Location 2 which is between locations 1 and 3 has a surface roughness of 61 nm which is an intermediate value between the highest and lowest roughness. This indicates that the heat dissipation rate is between the rates of locations 1 and 3. Even though location 2 is not adjacent to the periphery, it is relatively nearer to the periphery than location 3. Hence, the heat dissipation through the periphery is higher than location 3 and lower than location 1, resulting in intermediate surface quality.

This study reveals that morphological characteristics such as voids, debris, cracks, and other fractured components are not observed and hence, showing excellent surface characteristics. There is no significant change in topology in three locations (Figs. 14b, 15b, 16b). As briefly discussed in SEM analysis, the lesser the heat dissipation rate, the longer the heat stays on the surface. The magnitude of thermal stresses directly varies with the exposure of heat on the surface.

When the value of thermal stresses surpasses the mechanical strength of the material, surface defects (cracks, voids, debris, etc.) develop leading to an increase in surface roughness [22, 46]. The variation in the heat dissipation rate on different locations directly impacts the surface morphology of the specimen. Hence, it is observed
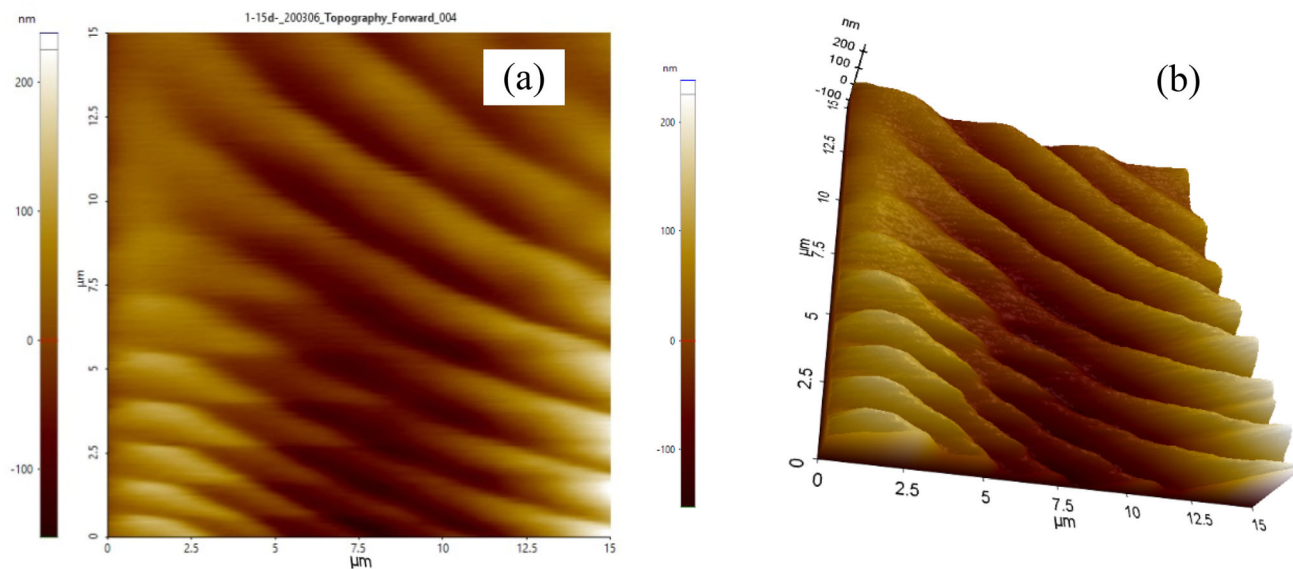
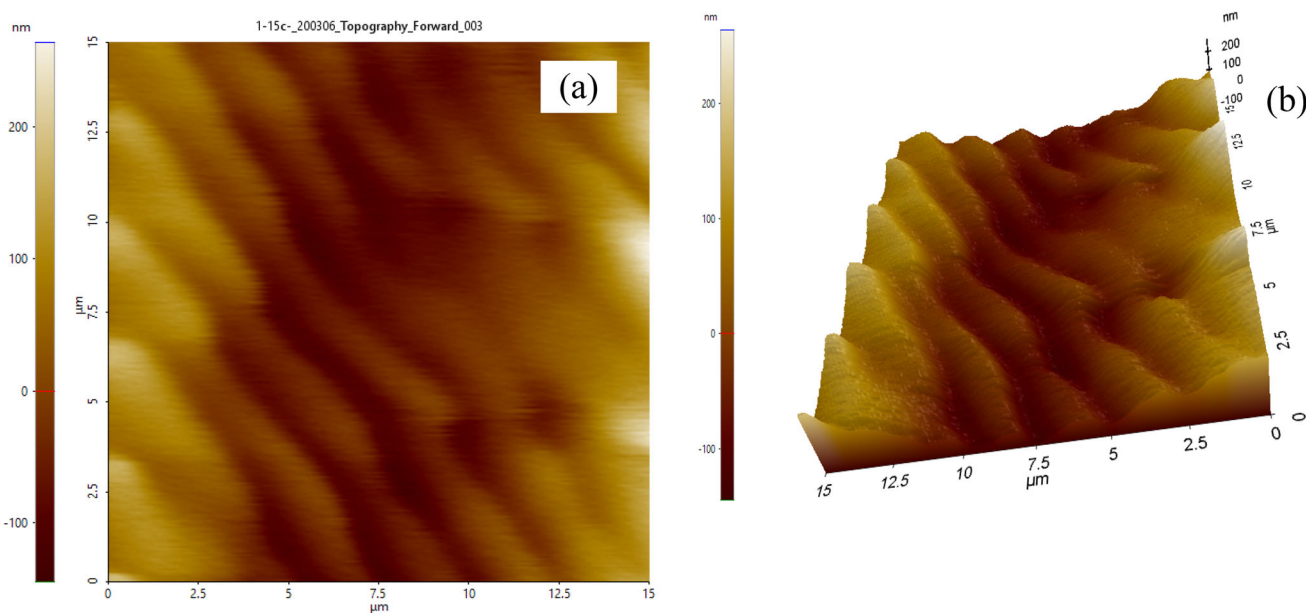**Fig. 14 a** Two-dimensional image of location 1 Ra = 46 nm, **b** topographic image of location 1

Fig. 15 a Two-dimensional image of location 2 Ra = 61 nm, **b** topographic image of location 2

that the surface roughness (in nm) decreases as it moves away from the center of the recast surface towards the periphery due to the increase in heat dissipation rate.

5 Conclusions

In the present research, the multi-objective optimization of WEDM parameters for the responses of micro-hardness and surface roughness is carried out through a hybrid ANN coupled GA technique to use WEDM as a post-processing technique in the SLM process. The process parameters used to optimize the WEDM process are the discharge current, discharge voltage, and pulse time-on. The key findings from the optimization are:

1. From the statistical analysis by ANOVA at a 95% confidence level, the discharge current is found to be the most influential factor that affects the micro-hardness and surface roughness.
2. From the five ANN models developed with the hidden neurons varying from 8 to 12, the 3–10–2 model is found to be the 'best-fit' neural architecture to be used for optimization using GA.
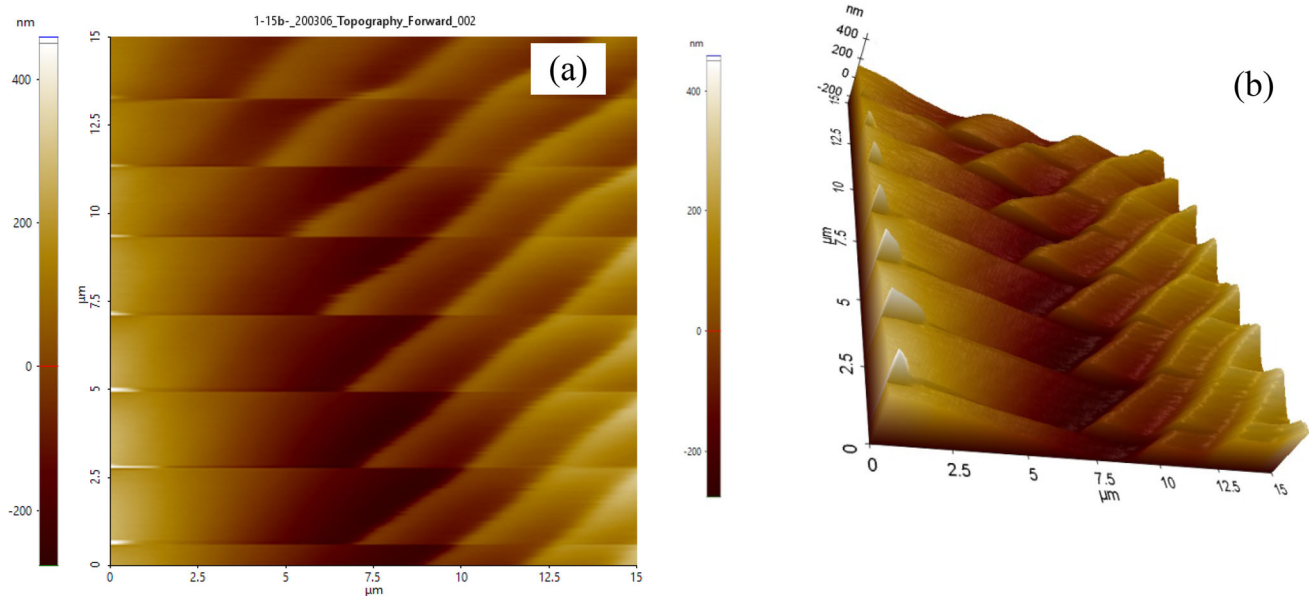
Fig. 16 **a** Two-dimensional image of location 3 Ra = 93 nm, **b** topographic image of location 3

3. The optimized process parameters are discharge current of 12 A, discharge voltage of 42 V, and pulse time-on of 12 μs for the maximized micro-hardness of 478 VHN and minimized surface roughness of 4.33 μm for the fitness function derived based on the results of the 3–10–2 ANN model.

4. A validation test results (micro-hardness: 492 VHN and surface roughness: 4.39 μm) show that the predicted results are in 98% agreement with the experimental data.

5. The white layer analysis shows that the increase in micro-hardness is proportional to the size of HAZ near the machining zone. In the recast surface, the poor surface quality (high Ra) is due to the presence of surface defects (e.g., cracks, voids, debris) formed by thermal stresses imposed by the drastic cooling rate experienced in the machining surface. The surface quality is improved (reduced Ra) up to 15.25% by the optimization studies.

6. The XRD analysis on the recast surface confirms the presence of Mg_2Si precipitation on the recast surface which increases the micro-hardness of the specimen. Also, it is understood that optimum parameters provide not only a better surface finish and higher micro-hardness but also a clean surface free from the deposition of the wire electrode material.

7. The AFM studies reveal that the surface integrity varies in different locations of the WEDMed surface. Voids, debris, cracks, and other fractured components are not evident confirming good surface characteristics. Further, the surface roughness (in nm) decreases as it moves away from the center of the recast surface toward the periphery due to the increase in the heat dissipation rate.

Hence, the ANN coupled genetic algorithm suggested is found to be an effective optimization tool to optimize WEDM parameters for post-processing of SLM–AlSi10Mg alloy resulting in maximum micro-hardness and minimum surface roughness with defect-free surfaces.

Authors' Contribution PV was involved in conceptualization, formal analysis, data curation, investigation, and writing—original draft. JJJ was involved in conceptualization, formal analysis, data curation, and writing—original draft. MP was involved in methodology, visualization, writing—review and editing, and supervision. TRP was involved in idea conception, validation, and writing—review and editing. NEP was involved in expert review, editing the manuscript, and technical guidance.

References

[1] Sames WJ, List F A, Pannala S, Dehoff R R, Babu S S. The metallurgy and processing science of metal additive manufacturing [J]. International Materials Reviews, 2016, 61:5, 315-360: 1-46.

[2] Wang P, Zhou H, Zhang L, Chen H, Zhu X, Lei H, Fang D. In situ X-ray micro-computed tomography study of the damage evolution of prefabricated through-holes in SLM-Printed AlSi10Mg alloy under tension [J]. Journal of Alloys and Compounds, 2020, 821, 1-8.

[3] Romano S, Abel A. *J Addit Manuf* (2019) p 394

[4] Arfan M, Yingfeng Z, Jingxiang L, Tao P, Zahid A, Altaf A. Investigation of T4 and T6 heat treatment influences on relative density and porosity of AlSi10Mg alloy components manufactured by SLM [J]. Computers & Industrial Engineering, 139, 2020, 1-16.

[5] Kugaevskii S, Pizhenkov E, Gamberga A. The effectiveness of additive SLM-technologies in the manufacture of cutting tools [J]. Materials Today: Proceedings, 2019, 19, 1977-81:1-5.

[6] Hadadzadeh A, Amirkhizb S, Sajad S, Kelly J, Li J, Mohammadi M. Microstructural investigation and mechanical behavior of a two-material component fabricated through selective laser melting of AlSi10Mg on an Al- Cu-Ni-Fe-Mg cast alloy substrate [J]. Journal of Additive manufacturing, 2020, 31, 1-36.

[7] Gianni N. Influence of rough as-built surfaces on smooth and Notched fatigue behavior of L-PBF AlSi10Mg [J]. Journal of Additive manufacturing, 2020, 34, 1-12.

[8] Rambabu P, Eswara Prasad N, Kutumbarao VV, Wanhill RJH. Aluminium alloys for aerospace applications [M]. Aerospace materials and technologies: vol. 1 –Aerospace Materials, Springer - IIM Book Series, Springer Nature Publications, Singapore, (2017) p 29

[9] Eswara Prasad N, Gokhales AA, Wanhill RJH. Aluminium - Lithium Alloys [M]. Aerospace materials and technologies: vol.1 – Aerospace Materials, Springer - IIM Book Series, Springer Nature Publications, Singapore, (2017) p 53

[10] Singh RK, Singh AK, Eswara Prasad N. Texture and Mechanical Property Anisotropy in an Al-Mg-Si-Cu Alloy [J]. Materials Science and Engineering A, Vol. A, 277, 2000 :114 – 122.

[11] Eswara Prasad N, Vogt D, Bidlingmaier T, Wanner A, Arzt E. High Temperature Low Cycle Fatigue Behaviour of an Aluminium Alloy (Al-12Si CuMgNi) [J]. Materials Science and Engineering A, Vol. A276, 2000: 283 – 287.

[12] Eswara Prasad N, Vogt D,Bidlingmaier T, Wanner A, Arzt E. Effect of Prior Fatigue Exposure on the Creep Behaviour of an Aluminium Alloy (Al-12Si-CuMgNi) [J]. Zeitschrift fur Metallkunde, Vol. 91, 2000:190 – 195.

[13] Eswara Prasad N, Vogt D, Bidlingmaier T, Wanner A, Arzt E. Low Cycle Fatigue and Creep – Fatigue Interaction in a Short Fibre-Reinforced Aluminium Alloy Composite [J]. Materials Science and Technology, Vol. 26, 2010: 1363 – 1372.

[14] Murthy CHVS, Anant Sagar DB, Eswara Prasad N. A Technical report on "the effect of heat treatment on microstructure and mechanical properties of nickel base cast superalloy supercast 247 A [J]. RCMA Technical Report No. RCMA (Mat.)/01/2013 (Restricted) p 181

[15] Amit K, Gobardhan L, Mahesh C, Eshwara Prasad N. Recent Development in Ellipsometry [C]// Proc National Seminar on Functional and Engineering Materials (FEM-2016), DESIDOC, New Delhi, (2016)

[16] Gibson I, DW Rosen, Brent S. Additive Manufacturing Technologies Rapid Prototyping to Direct Digital Manufacturing [M]. Springer Publications, 2010.

[17] M Azam, M Jahanzaib, JA Abbasi, M Abbas, A Wasim, S Hussain. Parametric analysis of recast layer formation in wire-cut EDM of HSLA steel [J].International Journal of Advanced Manufacturing technologies, 87, 2016: 713-722.

[18] J Yuan, K Wang, T Yu, M Fang. Reliable multi-objective optimization of high-speed WEDM process based on Gaussian process regression [J]. International journal of machine tools and manufacture, 2008, 48: 47-60.

[19] KH Ho, Newman ST, Rahimi Fard S, Allen R D. State of the art in wire electrical discharge machining (WEDM) [J]. International journal of machine tools & manufacture, 2004, 44, 1247-1259.

[20] Xiaoyu WU, Shujuan LI, Zhen JIA, Bin XIN, Xincheng YIN. Using WECM to remove the recast layer and reduce the surface roughness of WEDM surface [J]. Journal of Materials Processing Technology, 2019, 268: 140-148.

[21] Zhen Z, Hao H, Wuyi M, Zhong X, Yu H, Guojun Z. Study on machining characteristics of WEDM with ultrasonic vibration and magnetic field assisted techniques [J]. Journal of Materials Processing Technology, 2016, 234: 342-352.

[22] Maher I, Adsarhan A, Marashi H. Effect of Electrical Discharge Energy on White Layer Thickness of WEDM [J]. Comprehensive Materials Finishing, 2017, 1: 231-266.

[23] Yahya HSM, Abbas T, Amin NAS. Int J Hydrog Energy (2020) p 1

[24] Deshwal S, Kumar A, Chhabra D. CIRP J Manuf Sci Technol (2020) p 1

[25] Venkatesh P, Karthikeyan R. Comparative studies on modelling and optimization of hydrodynamic parameters on inverse fluidized bed reactor using ANN-GA and RSM [J]. Alexandria Engineering Journal, 2018, 57, 3019-32:1-14.

[26] Puviyarasan M, Senthil Kumar VS. An Experimental Investigation for Multi-Response Optimization of Friction Stir Process Parameters During Fabrication of AA6061/B_4C_p Composites [J]. Arabian Journal of Science and Engineering, 2015, 40, 1733–1741.

[27] TB Kumar, A Panda, GK Sharma, A Johar, Sougata Kumar KAR, Dharmendarbool C. Taguchi DoE and ANOVA: A systematic perspective for performance optimization of cross-coupled channel length modulation OTA [J]. 2020, 116, 153070: 1-10.

[28] H Abarghooei, H Arabi, S Hseyedein, B Mirzakhani. Modeling of Steady State Hot Flow Behavior of API-X70 Microalloyed Steel using Genetic Algorithm and Design of Experiments [J]. Applied Soft Computing Journal, 2017, 52, 471-477

[29] Ravindra B, Syam Sunder K, Siva Prasad T, Raju AVS, Eswara Prasad N. Int Manuf Sci Eng MSEC ASME, Notre Dame, Indiana, USA, (2012) p 503

[30] Babu P R, Ankamma Rao K, Eswara Prasad N. Burnishing of Engineering Materials [M]. Process Optimisation (DOE) and Maps, LAP LAMBERT Academic Publishing GmbH, Saarbrucken, Germany, (2012)

[31] Ravindra Babu P, Ankamma Rao K, Siva Prasad T, Raju AVS, Eswara Prasad N. Optimisation of Burnishing Parameters by DOE and Surface Roughness, Microstructure and Micro Hardness Characteristics of AA6061 Aluminium Alloy in T6 Condition [J]. International Journal of Engineering Research and Applications, Vol. 2, 2012: 1139-1146.

[32] Ravindra Babu P, Ankamma K, Siva Prasad T, Raju AVS, Eswara Prasad N. Optimisation of Burnishing Parameters and Determination of Select Surface Characteristics in Engineering Materials [J]. Academy Proceedings of Engineering Sciences, The Indian Academy of Science, 2012, 37: 503–520.

[33] Eswara Prasad N. Aluminium Alloy Ak 6 (Stampings) [M]. JSS 9630–16:2013, MSSC, MoD, GoI, New Delhi (2013)

[34] Mustafa A, Samet U, Bahattin ÇM. Performance and emission prediction of a compression ignition engine fuelled with biodiesel-diesel blends: A combined application of ANN and RSM based optimization [J]. Fuel, 2020, 269, 117472: 1-10.

[35] Shahbaz M, Taqvi SA, Loy ACM, Inayat A, Uddin F, Bokhari A. Artificial neural network approach for the steam gasification of palm oil waste using bottom ash and CaO [J]. Renewable Energy, 2019; 132: 243-54:1-46.

[36] Jha P, Kana EBG, Can SS, Nasrudin NA, Jewaratnam J, Hossain A, Ganeson PB. Performance comparison of feed forward neural network training algorithms in modelling microwave pyrolysis of oil palm fibre for hydrogen and biochar production [J]. Asia Pac J Chem Eng 2019; 15 (1):e2388: 1-16.

[37] Talebian-Kiakalaieh A, Amin NAS, Zarei A, Noshadi I. Transesterification of waste cooking oil by heteropoly acid

(HPA) catalyst: optimization and kinetic model [J]. Appl Energy, 2013,102:283-292.

[38] Kasmuri NH, Kamarudin SK, Abdullah SRS, Hasan HA, Som AM. Integrated advanced nonlinear neural network simulink control system for production of bio-methanol from sugar cane bagasse via pyrolysis [J]. Energy, 2019, 168:261-272.

[39] Nasrudin NA, Jewaratnam J, Hossain A, Ganeson PB. Performance comparison of feedforward neural network training algorithms in modelling microwave pyrolysis of oil palm fibre for hydrogen and biochar production [J]. Asia Pac J Chem Eng 2019; 15(1):e2388: 1-16.

[40] Shin Y, Kim Z, Yu J, Kim G, Hwang S. Development of NOx reduction system utilizing artificial neural network (ANN) and genetic algorithm (GA) [J]. J Clean Prod 2019; 232:1418-29.

[41] Prakash Maran LJ, Sivakumar V, Thirugnanasambandham K, Sridhar R. Artificial neural network and response surface methodology modeling in mass transfer parameters predictions during osmotic dehydration of Carica papaya [J]. Alex. Eng. J., 2013: 507–516.

[42] B Jiang, F Zhang, Y Sun, X Zhou, J Dong, L Zhang. Modeling and Optimization for curing of polymer flooding using an artificial neural network and a genetic algorithm [J]. J. Taiwan Int. Chem. Eng., 2014, 881: 1-8.

[43] Mcgeough JA. Electro Discharge Machining in Advanced Methods of Machining [M]. Springer: Dordrecht, 1988.

[44] H El-Hofy, Advanced Machining Processes [M], McGraw-Hill, 2005.

[45] C Wuet, X Wu, H Zhao, B Xu. Effect of sub-millimetre morphologies on the hydrophobicity of a copper surface prepared by WEDM [J]. Surface and Coatings Technology, 2020, 385, 125455:1-9.

[46] Y Wang, Z-X Li, S-W Yao, C-Z Wu. Analysis of discharge channel characteristics based on plasma flow and heat transfer in USV-MF complex assisted WEDM-LS [J]. International Journal of Heat and Mass Transfer, 2019, 150, 1-13.